Food and Bioprocess Technology (2024) 17:628–639
https://doi.org/10.1007/s11947-023-03156-4

RESEARCH

Edible Iron-Pectin Nanoparticles: Preparation, Physicochemical Characterization and Release Study

Ensi Gholam Jamshidi[1] · Farahnaz Behzad[2] · Mahdi Adabi[2,3] · Seyedeh Sara Esnaashari[1]

Received: 9 February 2023 / Accepted: 21 June 2023 / Published online: 1 July 2023

Abstract

Iron fortification in food is considered as an important way to prevent and treat iron deficiency. However, adding iron in food can affect flavor, color, and oxidation of fat components. Encapsulation of iron can solve the drawbacks of taste, color, and reactivity of iron in oral iron consumption without adverse effect on food quality. The aim of this work was to nanoencapsulate iron into pectin (Pec) nanoparticles (NP) by ion gelation method to prevent undesirable sensorial changes in foods and improve bioavailability of iron. The effect of different parameters including pectin concentration (Pec Con), $FeSO_4$ concentration (Fe Con), and volumetric ratio of Fe solution to Pec solution on iron loaded Pec nanoparticles (IP NP) size was investigated. Morphology, size, surface charge, and physicochemical features of the optimized particles were characterized. The iron released from IP NP was studied, and the mathematical model of release was extracted. Pec Con exhibited a direct effect on particle size. The optimized IP NP (Pec solution 0.1% (w/w), Fe solution 0.05% (w/w), and Pec/Fe: 2) had a hydrodynamic diameter of 417 nm with zeta potential of −11.7 mV and polydispersity index (PDI) of 0.13, with a nearly spherical morphology. Scanning electron microscopy (SEM) represented the mean size of 58 nm. Iron loading was about 7.5 ± 1.5%. FTIR results confirmed the interaction of iron ions with the hydroxyl and carboxyl groups of Pec. The results of differential scanning calorimetric (DSC) indicated the interaction of Pec with iron. The release profile of iron in all pH of 2, 6, and 7.4 showed a burst release at the beginning and then a sustained release occurred. In all three pH values, the mathematical model of release was Korsmeyer-Peppas with the highest R^2 value. Therefore, encapsulation of iron using pectin have a high potential to make nanoparticles with appropriate properties, which can be helpful for iron fortification of food.

Keywords Food fortification · Ion gelation · Iron loaded pectin nanoparticles · Nanoencapsulation

Introduction

Micronutrient deficiencies are a significant public health concern that affects vulnerable populations worldwide. Considering the fact that at least 60% of the world's population are affected by iron deficiency, it is one of the most prevalent micronutrient deficiencies throughout the world (Shilpashree et al., 2020). Iron deficiency leads to retarded growth and impaired cognitive perception in kids as well as poor health in adults (Kumari & Chauhan, 2022). Low consumption and poor bioavailability are the primary causes of iron deficiency anemia in industrialized nations. Besides, high intakes of iron-chelating compounds such as peppermint and turmeric or beverages like tea inhibit iron absorption (Saffarionpour & Diosady, 2021). In such conditions, food fortification with iron or iron supplements has been recommended as one of the preferred approaches (Min et al., 2016). Commercially available iron supplements are usually administered in multiple-dose regimens a day for high risk people, resulting in gastrointestinal (GI) adverse effects such as vomiting, constipation, diarrhea and abdominal cramps or pain. While iron-fortified foods provide a lower dose of iron into the GI tract at a time, it may actually help to reduce the risk of GI side effects. Although iron has various salt forms, including citrate, gluconate, ascorbate,

✉ Seyedeh Sara Esnaashari
s.esnaashari@iautmu.ac.ir

[1] Department of Medical Nanotechnology, Faculty of Advanced Sciences and Technology, Tehran Medical Sciences, Islamic Azad University, Tehran, Iran

[2] Department of Medical Nanotechnology, School of Advanced Technologies in Medicine, Tehran University of Medical Sciences, Tehran, Iran

[3] Food Microbiology Research Center, Tehran University of Medical Sciences, Tehran, Iran

oxide, fumarate, sulfate, or succinate (Hurrell, 2021), the most accessible and cost-effective form with acceptable solubility in water or diluted acid is $FeSO_4$ (Fe), which still remains in the first line of treatment (Patil et al., 2012; Bathla & Arora, 2022). However, iron atoms in Fe can readily react with other food ingredients, producing off-flavors, color alteration, and oxidation of fat components. For example, iron could react with unsaturated lipids (Kiskini et al., 2012) in food to produce rancidity, leading to change of the flavor and unacceptable color changes (Buyukkestelli & El, 2019). Also, undesirable color changes can result from interactions with anthocyanins, flavonoids, and tannins (Mehansho, 2006). In addition, polyphenols (compounds available in many plant-based food) can react with iron (Habeych et al., 2016). Therefore, adding iron without adverse effect on food quality is one of the most challenging issues. To succeed in the market, iron-fortified food should have desirable sensorial properties, which can be achieved by micro/nanoencapsulating ferrous ions to both maintain food quality and improve ferrous ion bioavailability. Targeting iron in GI using oral delivery involves several steps. First, the iron should be encapsulated using a suitable material that can protect it from degradation in the acidic environment of the stomach. This can be achieved using various materials such as lipids, proteins, or polysaccharides (Gharsallaoui et al., 2010; Hosny et al., 2015; Ghibaudo et al., 2018; Mohammadian et al., 2020; Bashir et al., 2022a, b). Once encapsulated, the iron should be delivered to the small intestine where it can be absorbed into the bloodstream. The small intestine is where most nutrient absorption takes place and has a more neutral pH than the stomach, making it a more favorable environment for iron absorption (Ghibaudo et al. 2018; Shubham et al., 2020). The encapsulated iron should then be released from its protective coating so that it can be absorbed by the body. This can be achieved through various mechanisms such as enzymatic degradation or pH-triggered release (Jash et al., 2022). Besides, encapsulation can inhibit direct exposure of ferrous ions to the gastrointestinal tract, and the gradual release can be profitable during its oral uptake (Katuwavila et al., 2016). Therefore, micro-/nanoencapsulation in the food industry can prevent deteriorating reactions between the encapsulated agents and food medium (Almasi et al., 2021; Jafari et al., 2017). Micro-/nanoencapsulation avoids the active ingredients from reacting with other components in food matrix and maintains its stability and functionality. As an example, ferric sodium EDTA as a suitable iron source for food fortification was encapsulated in W/O/W double emulsions to protect iron from undesirable interaction with food matrix. In this study, hydrophilic polymers including sodium caseinate and sodium alginate were used as emulsifier to provide higher stability and a controlled release system for iron (Saffarionpour & Diosady, 2022). In another study, magnesium was encapsulated via double emulsion and added to the cakes. The results indicated that magnesium encapsulated in double emulsion did not considerably affect the quality of cakes. Besides, the taste of cakes containing magnesium encapsulated in double emulsion was similar to magnesium free cakes. In addition, double emulsions had higher baking stability than control (Kabakci et al., 2021).

Nanoencapsulation has been accepted as carriers smaller than 100 nm in size (Jafari et al., 2017; Shin et al., 2015). In contrast to the conventional microencapsulation process in food industry, nanoscale capsules can provide further merits such as a higher surface-to-volume ratio resulting in more absorption in digestive tract, and they have a higher interaction with biological element like enzymes and receptors (Esfanjani et al., 2018). Moreover, using nanoparticles for nutraceutical delivery can reduce the dose of bioactive compounds due to their smaller size. Also, they have higher stability to pH variation and even more extended shelf life (Muthukrishnan, 2022).

Polysaccharides as abundant materials in nature, cost effective, and biodegradable have been used alone or in combination for encapsulation of several nutraceuticals such as resveratrol (Seethu et al., 2020), vitamin D (Jafari et al., 2019), eugenol (Wang et al., 2020), and folic acid (Assadpour et al., 2016). Pectin (Pec) is a natural polysaccharide, which is usually applied as a thickening agent in the food industry and as an oral dosage form because it is possible to be degraded by microbial enzymes of colon, leading to the release of encapsulated cargo at the targeted sites (Sriamornsak, 2011; Hosny et al., 2015). Pec has been used to microencapsulate sensitive polyunsaturated fatty acids (PUFA) via spray drying as well. PUFA droplets, coated with Pec in combination with pea protein isolate (PPI), demonstrated the best oxidative protection compared to the control group and PPI encapsulated samples (Aberkane et al., 2014). Pec consists of poly-D-galacturonic acid linked via α-1,4-glycosidic bond, and the presence of side chains of galactose, arabinose, and rhamnose gives the chance of using the ion gelation method with divalent cations for micro-/nanocapsules of Pec. Jacob et al. (2020) prepared Pec NP with magnesium ions as a divalent cross linker through ion gelation method, which were biocompatible with THP-1 cells. Spherical iron-pectin beads (1–2 mm) were also made with Fe. Higher iron transport over Caco-2/TC7 cells monolayers was achieved by iron-pectin beads compared to the Fe control group (Ghibaudo et al., 2018). Jonassen et al. (2013) also reported that ionically cross-linked Pec NP can be produced by zinc chloride with Pec in the presence of sodium chloride.

Iron encapsulation into Pec is necessary for several reasons: (1) iron is a reactive metal that can easily oxidize and form insoluble compounds in the presence of oxygen and

moisture. Encapsulation in Pec protects iron from oxidation and degradation, ensuring its stability and bioavailability; (2) encapsulation allows for the controlled release of iron over the time, which can improve its absorption and utilization by the body; (3) iron supplements often have a metallic taste and odor that can be unpleasant for some people. Encapsulation in Pec can mask these sensory properties, making the supplement more palatable; (4) iron encapsulated in Pec improves solubility in water, which can enhance its bioavailability and absorption by the body (Gupta et al., 2015; Shubham et al., 2020). Considering the significance of Pec as a carrier for oral route both in food fortification and pharmaceutical industry, the goal of the current research was to develop IP NP through ion gelation process. In the formulation, Fe was used as a cross-linking agent, and its encapsulation was carried out using Pec NP. IP NPs were physico-chemically characterized by SEM, FTIR, DLS, and DSC. The loading capacity was decided by UV-Visible spectrophotometry. To simulate the release kinetics of iron from IP NP in the GI tract, buffer solutions with different pH values including pH 1.2 for the stomach, pH 6 for the intestines, and pH 7.4 for the biological body fluids were applied. The mathematical model of release behavior was determined as well.

Materials and Methods

Materials

Pec from citrus peel (polygalacturonic acid ≥ 65%) was purchased from Hanit, Vienna, Austria. Phenanthroline-1,10 was bought from Merck. The dialysis bag was from Sigma Company. Deionized water was utilized in all the experiments. Other materials were analytical grade.

Apparatus

The ultraviolet-visible (UV-Vis) spectrophotometer (CECIL, model CE 1021) was used. The size and shape of NP were evaluated by scanning electron microscope (SEM) techniques using Cambridge (S360). Fourier transform infrared spectroscopy (FTIR) measurements (Shimadzu (8400s)) were performed in the range of 4000–500 cm^{-1}. The zeta potential (ζ) and size distribution were determined by Zetasizer (Malvern, model Nano-ZS) and dynamic light scattering (DLS) (Scatter and Scope, model Scatter Scope II). In addition, centrifuge was exerted using a model-universal. Differential scanning calorimetry (DSC) and heater stirrer were recorded by TA (Q100) and (Heidolph, model Kera-Disk), respectively.

Methods

Preparation of IP NP

IP NPs were prepared using the ion gelation method as described by Jacob et al. with slight modifications using $FeSO_4$ as the divalent cation (Jacob et al., 2020). Different concentrations (Cons) of Pec solution (0.05, 0.1, 0.15, and 0.2 w/w) in 0.05 M of NaCl solution were prepared on the magnetic stirrer. Then, Fe solution was dissolved in deionized (DI) water with different Cons according to the Table 1 (0.05, 0.025, 0.075, and 0.1 w/w). These Cons for Pec solution and Fe solution were determined by preliminary studies. Using 0.45 µm and 0.22 µm filters, all of the solutions previously stated were filtered for eliminating the impurities. The Pec solution was maintained under magnetic stirring at 500 rpm and 25 °C, and then the iron solution was dropwise added by a syringe pump (160 µl.min^{-1}) and stirred for further 90 min. The volumetric ratio of Pec solution to iron solution (Pec/Fe) was 1, 2, 3, and 4. The NP obtained were collected by centrifugation at 10,732 g for 30 min at 4 °C and washed twice with DI. The size of the IP NP obtained was measured by DLS. At last, the optimized sample (Pec solution 0.1% (w/w), Fe solution 0.05% (w/w) and Pec/Fe: 2) was freeze-dried and used for further characterizations. It should be noted that the optimized sample was selected based on the smallest size with narrow distribution.

Characterization of IP NP

The Measurement of Size and Zeta Potential

DLS was used to investigate the size (d_{50}) of NPs (scatterscope1, K-ONE, S. Korea). The size distribution was

Table 1 Different amounts of Pec, Fe, and the Pec/Fe in the production of IP NP

Run	Factor 1 A:Pec Con (w/w%)	Factor 2 B:Fe Con (w/w%)	Factor 3 C:Pec/Fe
1	0.05	0.05	2
2	0.1	0.05	2
3	0.15	0.05	2
4	0.2	0.05	2
5	0.1	0.025	2
6	0.1	0.05	2
7	0.1	0.075	2
8	0.1	0.1	2
9	0.1	0.05	1
10	0.1	0.05	2
11	0.1	0.05	3
12	0.1	0.05	4

reported as poly dispersity index (PDI) and determined through $(\frac{SD}{Mean})^2$ formula (SD as standard deviation and mean as average diameter of the NP) (Esnaashari et al., 2020). The amount of particle charge was determined by a Zetasizer (Nano-ZS, Malvern Instruments Ltd., UK) ($n=3$).

Fourier Transform Infrared Spectroscopy (FTIR) Spectroscopy

In order to investigate the chemical interaction between iron and other components of the formulation, the FTIR analysis was performed in neutral atmosphere. FTIR spectroscopy (Shimadzu FTIR-8400S) absorption spectra were assessed with the wavelength range of 4000–500 cm^{-1}, utilizing transparent KBr pellets of Pec, Fe, and IP NP at room temperature.

Differential Scanning Calorimetric (DSC) Analysis

DSC was used to investigate the crystal structure or amorphous state. In this regard, a certain amount of Fe, Pec, and IP NP was placed in the sample container of the device (TA (Q100)). The analysis was performed in the heat flow range from 25 to 250 °C (heating rate 10 °C/min) in a nitrogen gas atmosphere with a flow rate of 25 mL/min (Hatefi & Farhadian, 2020).

Scanning Electron Microscopy (SEM) Analysis

The size, shape, and surface morphology was characterized by SEM (Cambridge (S360)). IP NP suspension was first dried on the foil at room temperature. The samples were then coated with gold (Au) under an argon atomosphere and were investigated by a SEM with at an accelerating voltage of 20 kV. The mean particle size was determined by measuring approximately 40 NPs by SemAfore software (version 5.21, JEOL) (Esnaashari & Amani, 2018).

Standard Calibration Curve of Fe by the UV-Vis Spectrophotometer

To investigate the amount of iron in release test and the amount of loading percentage, the derivation method via 1,10-phenanthroline was applied because it forms a complex with iron ions, which has a characteristic absorption peak in UV-V is spectroscopy. At this stage, both reducing solution and chromogen solution were used. For 1,10-phenanthroline assay, the following solutions have been prepared (Pitarresi et al., 2008):

1. The reducing solution contained 12.5 ml of HCl and 5.5 g of ascorbic acid adjusting the ultimate volume at 500 mL with DI water. Ascorbic acid was used as a reducing agent because it reduces Fe^{+3} to Fe^{+2}, and then 1,10-phenanthroline will have a complex with Fe^{+2}.
2. The chromogen solution was prepared by combining 68 g of sodium acetate and 45 mg of 1,10-phenanthroline in 250 mL of DI water.

To draw the calibration curve for Fe Con, 1 mL of Fe solution with certain Con was added to 1 mL of reducing solution. After 30 min, 1 mL of chromogen solution was added, and UV-Visible absorption was read at $\lambda=411$ nm (Pitarresi et al., 2008).

The Measurement of Encapsulation Efficency and Iron Loading

Aliquots (10 mg) of IP NP powder were dissolved in 2 mL of 1 N HCl solution to disintegrate the IP NP and release the loaded iron. Samples were filtered after 24 h. To calculate the amount of released iron, the filtered solutions were exposed into reducing and chromogen solutions as mentioned. The iron loading capacity and encapsulation efficiency were determined by the following equations (Esnaashari & Amani, 2018):

$$\text{Encapsulation efficency } \% = \frac{\text{amount of iron in IP NPs (mg)}}{\text{initial amount of iron (mg)}} \times 100$$

$$\text{Iron loading capacity } \% = \frac{\text{amount of iron in IP NPs (mg)}}{\text{amount of IP NPs (mg)}} \times 100$$

Release Study

To investigate the release profile of the iron from the formulation, a certain amount of the IP NP powder containing a certain amount of iron mass was dispersed in 2 mL of DI water and then placed in a dialysis bag (cut off of 12 kDa). Then, the dialysis bag containing the NP solution was placed in the medium containing phosphate buffered saline (PBS) at pH 2, 6, and, 7.4 in a shaker incubator (37 °C, 100 rpm). At specified intervals, the entire media which is surrounding the dialysis bag was replaced with a similar amount of fresh medium. The Con of the Fe released in the substituted medium was measured by a UV-Vis spectrophotometer at $\lambda=411$ nm. The cumulative release percentage curve of iron versus time was plotted. All of the experiments were repeated three times.

Fitting the Mathematical Formulations for Iron Release

The mechanism of iron release from IP NP was determined by using various mathematical models. The iron release data was fitted to mathematical models including zero-order,

first-order, and second-order equations, as well as the Korsmeyer–Peppas model, Higuchi, Weibull, and Hixson-Crowell. The values of R^2, Akaike information criterion (AIC), and BIC were calculated. The best fitted model had the largest R^2 value. All the mathematical calculations were performed through an open access curve fitting software (KinetDS 3 rev 2010) (Esnaashari & Amani, 2018; Katuwavila et al., 2016).

Results and Discussions

DLS and Zeta Potential Analysis

IP NPs were prepared through the ion gelation method since Pec as a negatively charged polymer can be cross-linked with divalent cations of various elements such as zinc (Jonassen et al., 2013), magnesium (Jacob et al., 2020), and iron (Ghibaudo et al., 2018). Pec chains have an elongated structure in distilled water due to the negative charge repulsion between the polymer chains. To remove these negative charge and improve salting out process for Pec NP formation, NaCl solution (0.05 M) was used (Chittasupho et al., 2013; Jonassen et al., 2013). Positive charge polymers can also interact with negative charge of Pec. Nanoencapsulation of folic acid was performed through a double emulsion while pectin in combination with whey protein concentrate (WPC) constituted the outer aqueous phase (Assadpour et al., 2016). In the present work, Fe was used as a source of iron cation to participate in the ion gelation process and was simultaneously encapsulated in Pec NP. Thus, some of the effective parameters on IP NP' size in ion gelation method including Pec Con, Fe Con, and Pec/Fe were studied. As depicted in Fig. 1a, the size of the particles enhanced as Pec Con increased from 0.05% (270 nm) to 0.2% (w/w) (541 nm). However, the size of particles did not follow a constant trend by increasing the Fe con and Pec/Fe (Fig. 1b, c). The optimized sample (Fe Con:0.1, Pec Con: 0.05, and Pec/Fe:2) showed a hydrodynamic diameter of 417 nm and acceptable PDI of 0.13, representing a narrow size distribution (Fig. 2a). Previous studies also reported similar size for Pec NP. In addition, they claimed that Pec Con had a direct effect on Pec NP size (Jacob et al., 2020; Opanasopit et al., 2008; Yan et al., 2017).

The zeta potential of IP NP was about -11.7 ± 0.2 mV (Fig. 2b). Negative charge of the particles was due to the unreacted carboxyl groups covered IP NP surface (Jacob et al., 2020). Since freeze-dried powder of IP NP showed a good dispersibility and stability in water, it seems that IP NP took the advantage of steric rather than electrostatic stability. This spatial hindrance can be the result of superficial carboxyl group hydration in Pec polymer chains.

SEM Analysis

The size, shape, and surface morphology of the optimized sample was characterized by the SEM. The results indicated that the particles were irregular and relatively spherical in shape and had an average particle size of 58 ± 19 nm (Fig. 3). The tremendous difference in determination of size

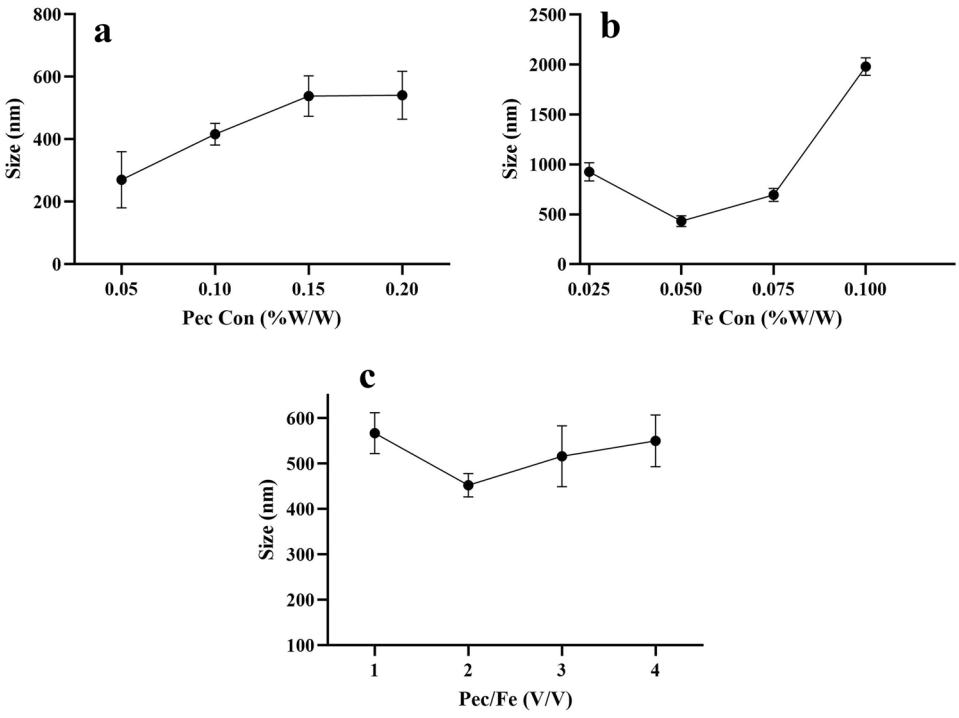

Fig. 1 The effect of different Cons of **a** Pec (w/w%) with Fe 0.05 (w/w%), Pec/Fe 2 (v/v) **b** Fe (w/w%) with Pec 0.1 (w/w%), Pec/Fe 2 (v/v), and **c** Pec/Fe (v/v) with Fe 0.05 (w/w%), Pec 0.1 (w/w%) on the size of particles

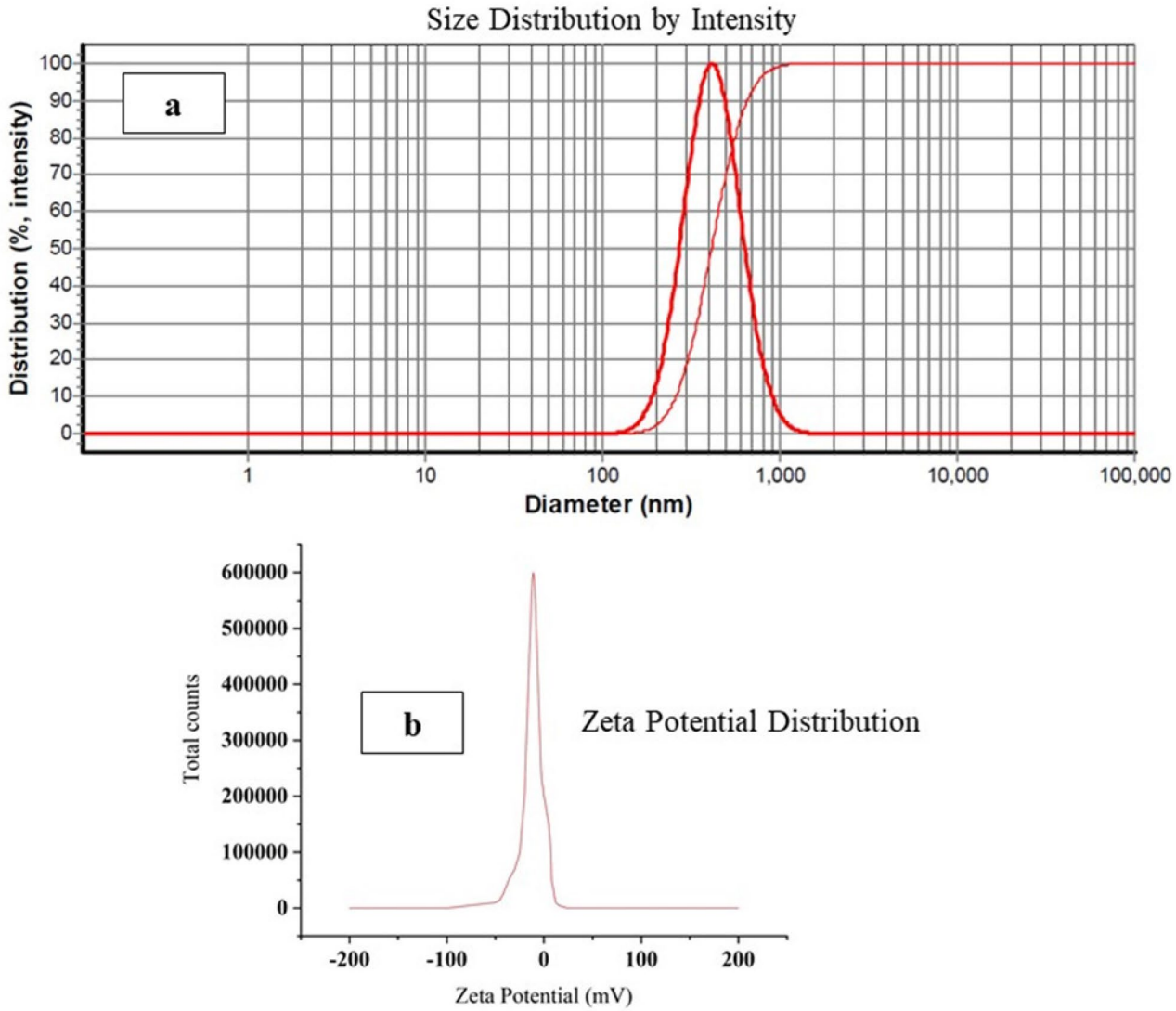

Fig. 2 Size distribution and zeta potential distribution of IP NP for the optimized sample (Pec Con:0.1, Fe Con: 0.05, and Pec/Fe:2)

for IP NPs between DLS and SEM is related to the bibulous feature of Pec which causes highly hydrated form in water, but its structure is shrinked in dry situation (Yu et al., 2009).

FTIR Spectroscopy

The FTIR spectra can verify the surface groups of materials and the possible interaction between them. The FTIR spectra of Pec, Fe, and IP NP are depicted in Fig. 4. The presence of iron in NP was revealed by the FTIR spectra. The results obtained from the Pec spectrum showed a band about 3400 cm^{-1} related to the stretching vibration of the O–H groups. Of course, the band in this range may also be related to the remaining moisture in the sample (Adabi et al., 2011). It is not possible to totally eliminate the moisture because Pec absorbs water easily (Boanares et al., 2018, Dekkers et al., 2018). Besides, the C-H and C = O groups caused the stretching bands about 2930 cm^{-1} and 1730 cm^{-1}, respectively in the structure of Pec (Jacob et al., 2020). The peak about 770 cm^{-1} are due to C-H bending vibration (Joel et al., 2018). The spectrum of ferrous sulfate, with four bands observed about 3250 cm^{-1}, 1500 cm^{-1}, 1080 cm^{-1}, and 820 cm^{-1}, is in agreement with the results of Bryszewska (2019). The spectra of IP NP preserved approximately much of the absorption bands attributed to its components with small shifts. A band (about 1090 cm^{-1}) which is attributed to sulfate groups can be observed in the spectra of NP with small shifts.

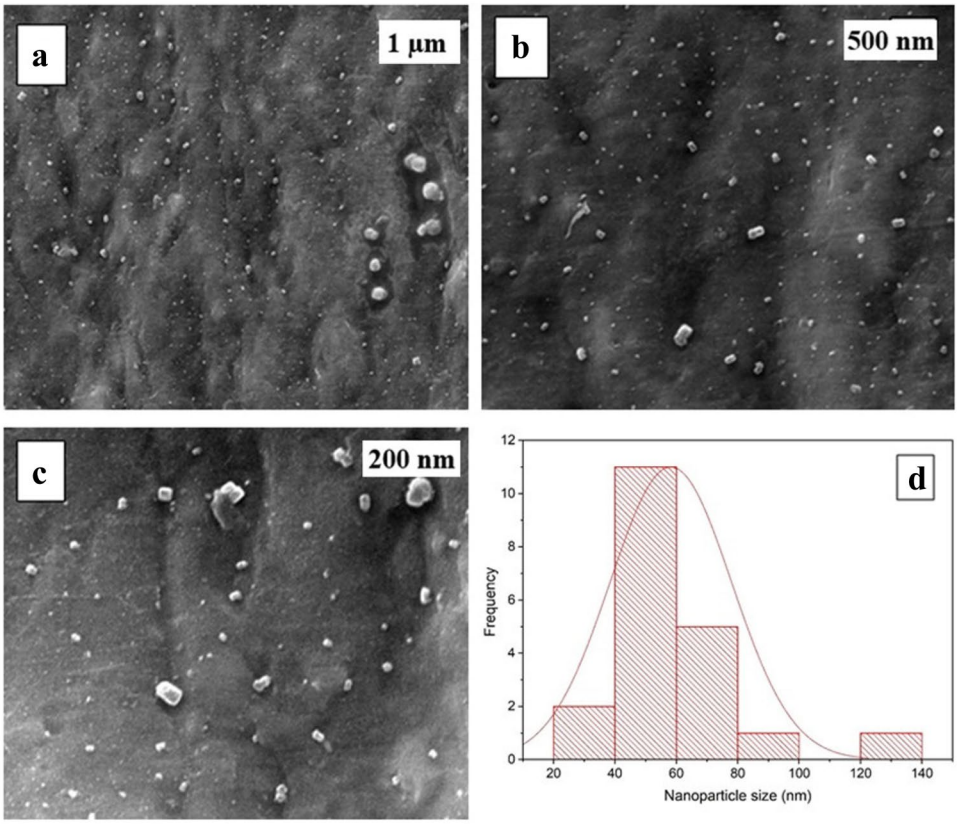

Fig. 3 The SEM image of the morphology of IP NP and a particle size distribution histogram

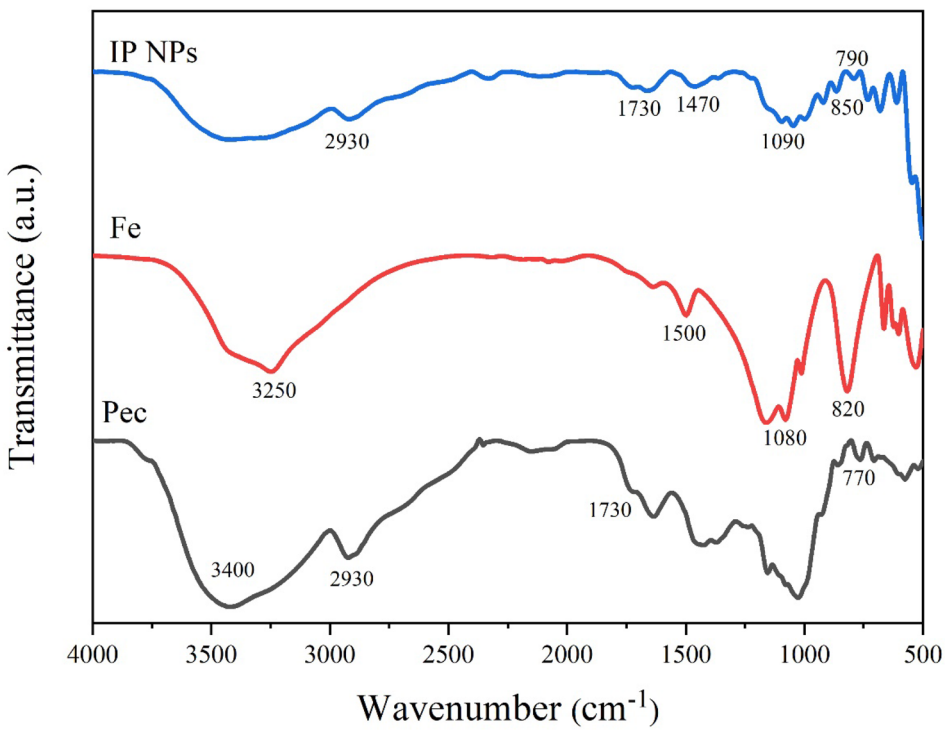

Fig. 4 FTIR analysis of Pec, Fe, and IP NP

DSC Analysis

DSC measures the change in the heat capacity as the polymer matrix changes from a glassy state to a rubbery state, known as glass transition temperature (Tg) (Hatefi & Farhadian, 2020; Perumal et al., 2018). The Tg depends upon intermolecular interactions, the chain flexibility, molecular weight, and branching and cross-linking density (Chaichi et al., 2017). In Fig. 5, the DSC of Pec shows a board peak about 70–100 °C, which is attributed to the Tg temperature of Pec. In addition, it can be related to water evaporation (Mishra et al., 2008; Nawrocka et al., 2017). The peak of ferrous sulfate appeared at 126 °C (Yu et al., 2013). Also, nanoparticle sample indicates the presence of Pec and Fe.

Encapsulation Efficiency and Iron Loading

To determine the amount of released iron and quantify encapsulation efficiency and iron loading capacity of IP NP, the standard calibration curve of Fe at $\lambda = 411$ nm (Pitarresi et al., 2008) was depicted in Fig. 6 ($Y = 0.0053X + 0.1985$, R^2 value = 0.9776). The encapsulation efficiency and iron loading capacity of IP NP were about $73 \pm 4\%$ and $7.5 \pm 1.5\%$ ($n = 3$), respectively. Iron loading capacity for chitosan and Eudragit microcapsules was reported as 2.8–5.3% (w/w) and 1.7–9.6% (w/w), respectively (Pratap Singh et al., 2018), which was close to our study.

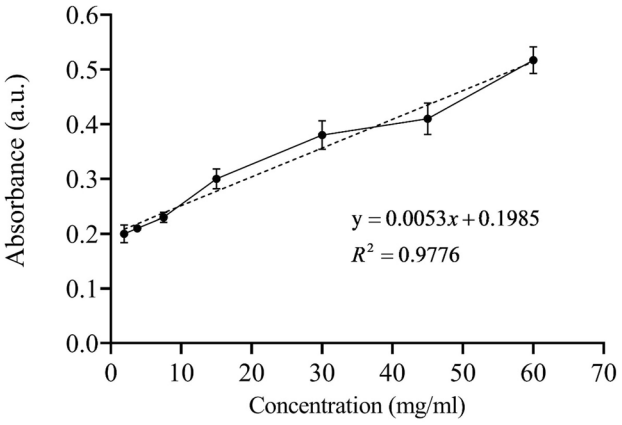

Fig. 6 Standard calibration curve (Con vs absorbance) of ferrous sulfate

Release Study

The in vitro release of iron from IP NP in buffer solutions with different pH values (pH 2, 6, and 7.4) is shown in Fig. 7. These pH values simulate various conditions that IP NP experience in vivo.

As expected, an initial burst release (40%) of iron from Pec NP can be observed in pH 6 and 7.4, whereas it was about 70% in pH 2 values during 10 h, which could be ascribed to the iron ions attached to the Pec NPs surface. In pH 2, the

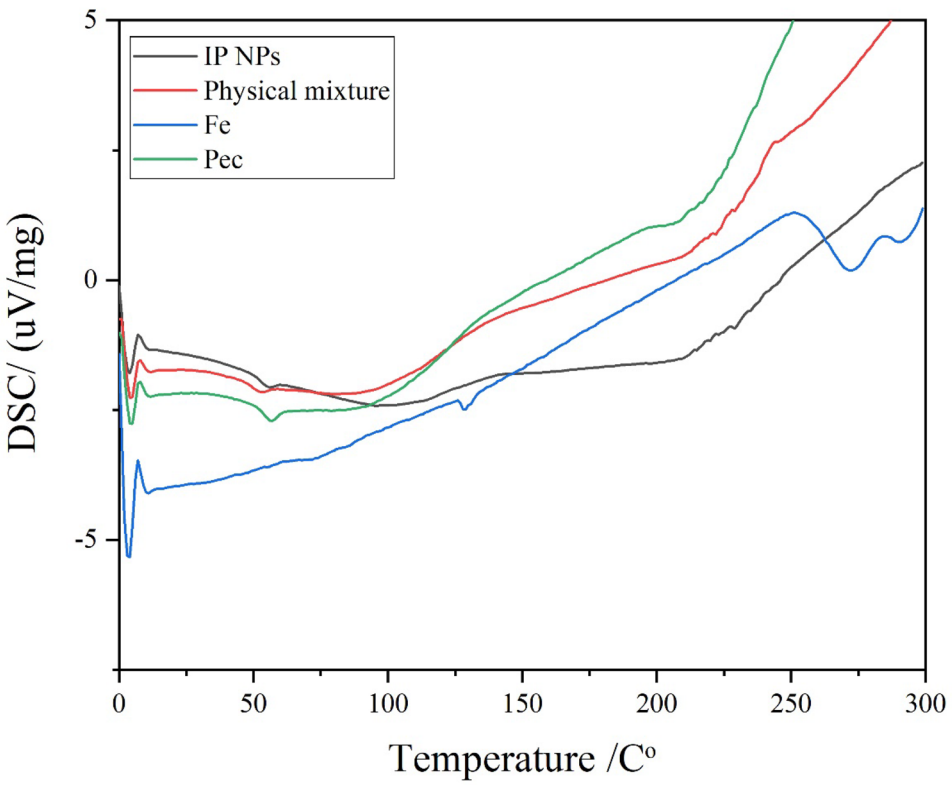

Fig. 5 DSC curve of Pec, Fe, and IP NP

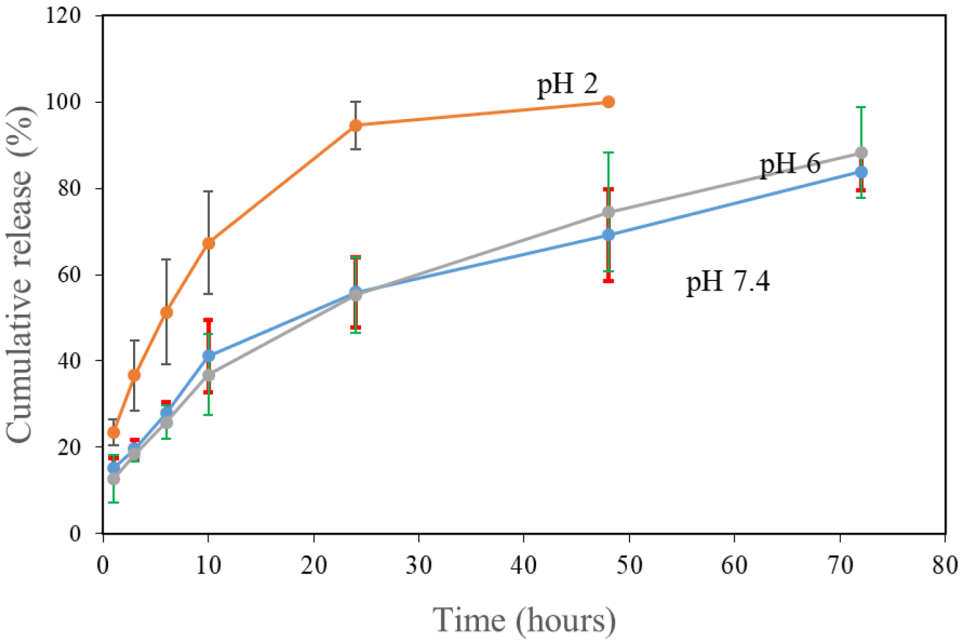

Fig. 7 Cumulative release of IP NP at predetermined time intervals in pH values of 2, 6, and 7.4 buffer solutions

rate of iron releasing was more, rapid and about 100% of iron was released during 50 h. In contrast, in pH 6 and 7.4, the initial burst release was slower, and around 85% of the iron attached to Pec NPs was released after 72 h. Therefore, it can be claimed that the total amount of iron released from Pec NP at pH 2 was around 40% in the stomach, while a sustained release pattern can be occurred in the intestine. According to Katuwavila et al. (2016), the release of 65–70% iron in an intestinal pH values of 6 and 7.4 is favorable for oral delivery formulations since iron absorption predominantly occurs in the duodenum. In Pratap Singh et al. (2018) study, total iron release from chitosan and Eudragit microcapsules approximately happened within 2 h in pH of 1, which indicates the iron bioavailability in the stomach. Besides, in pH of 4, about 67–94% and 53–70% of iron were released in 2 h for chitosan and Eudragit microcapsules, respectively. In pH of 7, which is used to simulate food soaking/cooking/processing in water and also human saliva, 10–18% of iron from chitosan and 12–25% iron from Eudragit particles were released. In comparison, the applied pH in our work was slightly different (pH of 2, 6, and 7.4) from the Pratap Singh study, which can affect iron release profile. Although, chitosan and Eudragit microcapsules were suitable for iron delivery in food with mild pH, in case of acidic food products, IP NP would be a better choice, due to the slower release rate in pH of 2 and 6.

The release behavior of iron from IP NP was also investigated through various mathematical models including zero, first, and second orders, Higuchi, Korsmeyer–Peppas, Weibull, and Hixson–Crowell models. The best fitted model will have the closest R^2 value to unity. In all three pH values of 2, 6, and 7.4, the best fitted model was Korsmeyer-Peppas with the highest R^2 value of 0.97590, 0.99372, and 0.98384, respectively (Table 2). Pratap Singh et al. (2018) found out that the Higuchi model and Hixson-Crowell model were the best fitted one for the release of iron from chitosan and Eudragit microcapsules. Their findings suggested that iron release was governed by diffusion through coating material, and the dissolution phenomenon caused a size reduction of the capsules. Difference in iron release model from IP NP compared to chitosan and Eudragit microcapsules can be the results of size scale. IP NP had hydrodynamic diameter of 417 nm, while its size in SEM image was about 58 ± 19 nm. Chitosan and Eudragit microcapsules had 3–5 μm size in SEM images, which should be much more in suspension state. In order to determine the mechanism of release from the particles in the Korsmeyer-Peppas model, it is necessary to calculate the "n" value in this formulation. Regarding spherical particles, when $n \leq 0.43$, it shows a Fickian diffusion, but when $0.43 < n < 0.85$, it shows a non-Fickian release that indicates the drug is released from hydrophilic polymer components (Keawchaoon & Yoksan, 2011; Motwani et al., 2008). In the present work, n value is 0.39 at pH 2, 0.47 at pH 6, and it is equal to 0.41 in pH 7.4.

Table 2 Statistical analyses of mathematical models of release at pH values of 2, 6, and 7.4

	Name	R^2	AIC	BIC	RMSE
pH 2					
Zero order		0.7838	45.639	45.223	13.11
First order		0.6554	49.7021	49.2856	18.405
Second order		0. 49,737	61.106	60.690	47.6082
Higuchi	y = K*t^(1/2)	0.68999	47.8040	47.3875	1.5712
Korsmeyer-Peppas		0.97590	38.3374	37.9209	7.13901
weibull		0.85250	43.0554	42.6390	10.577
Hixson-Crowell	y = [K*(t-lag) + C0^(1/3)]^3	0.703879	50.0383	49.4136	16.0223
Hill equation		0.51655	53.4368	53.0203	25.1248
pH 6					
Zero order		0.93904	44.080	43.972	6.6188
First order		0.78567	54.570	54.46	14.001
Second order		0.57021	101.15	101.04	390.17
Higuchi	y = K*t^(1/2)	0.98970	31.628	31.520	27.197
Korsmeyer-Peppas		0.99372	23.216	23.108	14.912
weibull		0.97924	32.686	32.578	2.9332
Hixson-Crowell	y = [K*(t-lag) + C0^(1/3)]^3	0.84785	50.5116	50.403	10.478
Hill equation		0.9409	40.451	40.343	5.1077
pH 7.4					
Zero order		0.9144	44.953	44.845	7.0447
First order		0.76559	52.733	52.624	12.280
Second order		0.58388	78.542	78.433	77.593
Higuchi	y = K*t^(1/2)	0.9066	45.560	45.452	7.3572
Korsmeyer-Peppas		0.98384	30.121	30.012	2.4420
weibull		0.97731	32.0442	31.9361	2.8016
Hixson-Crowell	y = [K*(t-lag) + C0^(1/3)]^3	0.82231	49.607	49.499	9.8229
Hill equation		0.95195	37.264	37.156	4.0676

AIC Akaike information criterion, *BIC* Bayesian information criterion or Schwarz criterion, *RMSE* root mean squared error

Conclusion

Iron deficiency is still a global challenge, and iron-fortified foods can be a reasonable and desirable route of administration. However, iron is known to react with oxygen, which can affect the quality of food products. Encapsulating iron into Pec can prevent its oxidation and improve the shelf life of food products. We successfully developed a powder form of iron loaded IP NP through the ion gelation method and freeze-dried. Investigating the operational parameters showed that IP NP with a hydrodynamic diameter of 417 nm and size of 54 nm of dried form were achieved with Pec Con 0.1, Fe Con 0.05, and Pec/iron ratio of 2. The loading capacity was about 7.5 ± 1.5%. The release study of iron from IP NP in various pH (2, 6, and 7.4) revealed that about 40% of loaded iron was released in the stomach, but it would have sustained trend in the intestine. Therefore, IP NP can be a desirable choice for food fortification due to ease of preparation process and cost effectiveness. In addition, iron encapsulation into Pec and developed powder form can improve stability. However, further studies are needed to optimize the encapsulation process and investigate the long-term effects of encapsulated iron on human health. Additionally, more research is needed to explore the potential of using other natural polymers for encapsulation and their effects on iron availability.

Acknowledgements We thank the Tehran Medical Sciences, Islamic Azad University for supporting this project.

Author Contribution Ensi Gholam Jamshidi: investigation, Farahnaz Behzad: writing—original draft, Mahdi Adabi: conceptualization, writing—review and editing, Seyedeh Sara Esnaashari: conceptualization, writing—review and editing, supervision.

Data Availability All data generated or analyzed during this study are included in this manuscript.

Declarations

Conflict of Interest The authors declare no competing interests.

References

Aberkane, L., Roudaut, G., & Saurel, R. (2014). Encapsulation and oxidative stability of PUFA-rich oil microencapsulated by spray drying using pea protein and pectin. *Food and Bioprocess Technology, 7*1505–1517.

Adabi, M., Saber, R., Adabi, M., & Sarkar, S. (2011). Examination of incubation time of bare gold electrode inside cysteamine solution for immobilization of multi-walled carbon nanotubes on a gold electrode modified with cysteamine. *Microchimica Acta, 172*(1), 83–88.

Almasi, K., Esnaashari, S. S., Khosravani, M., & Adabi, M. (2021). Yogurt fortified with omega-3 using nanoemulsion containing flaxseed oil: Investigation of physicochemical properties. *Food Science & Nutrition, 9*(11), 6186–6193.

Assadpour, E., Maghsoudlou, Y., Jafari, S.-M., Ghorbani, M., & Aalami, M. (2016). Evaluation of folic acid nano-encapsulation by double emulsions. *Food and Bioprocess Technology, 9*(12), 2024–2032.

Bashir, O., Bhat, S. A., Basharat, A., Qamar, M., Qamar, S. A., Bilal, M., & Iqbal, H. M. (2022a). Nano-engineered materials for sensing food pollutants: Technological advancements and safety issues. *Chemosphere, 292,* 133320.

Bashir, O., Rashid, S., Masoodi, N., Khan, S. A., Majid, I., & Malik, M. (2022b). *Nanocellulose: Chemistry, preparation, and applications in the food industry* (pp. 155–177). Elsevier.

Bathla, S., & Arora, S. (2022). Prevalence and approaches to manage iron deficiency anemia (IDA). *Critical Reviews in Food Science and Nutrition, 62*(32), 8815–8828.

Boanares, D., Ferreira, B., Kozovits, A., Sousa, H., Isaias, R., & França, M. (2018). Pectin and cellulose cell wall composition enables different strategies to leaf water uptake in plants from tropical fog mountain. *Plant Physiology and Biochemistry, 122,* 57–64.

Bryszewska, M. A. (2019). Comparison study of iron bioaccessibility from dietary supplements and microencapsulated preparations. *Nutrients, 11*(2), 273.

Buyukkestelli, H. I., & El, S. N. (2019). Development and characterization of double emulsion to encapsulate iron. *Journal of Food Engineering, 263*, 446–453.

Chaichi, M., Hashemi, M., Badii, F., & Mohammadi, A. (2017). Preparation and characterization of a novel bionanocomposite edible film based on pectin and crystalline nanocellulose. *Carbohydrate polymers, 157*, 167–175.

Chittasupho, C., Jaturanpinyo, M., & Mangmool, S. (2013). Pectin nanoparticle enhances cytotoxicity of methotrexate against hepG2 cells. *Drug Delivery, 20*(1), 1–9.

Dekkers, B. L., Hamoen, R., Boom, R. M., & van der Goot, A. J. (2018). Understanding fiber formation in a concentrated soy protein isolate-pectin blend. *Journal of Food Engineering, 222*, 84–92.

Esfanjani, A. F., Assadpour, E., & Jafari, S. M. (2018). Improving the bioavailability of phenolic compounds by loading them within lipid-based nanocarriers. *Trends in Food Science & Technology, 76*, 56–66.

Esnaashari, S. S., & Amani, A. (2018). Optimization of noscapine-loaded mPEG-PLGA nanoparticles and release study: A response surface methodology approach. *Journal of Pharmaceutical Innovation, 13*(3), 237–246.

Esnaashari, S. S., Muhammadnejad, S., Amanpour, S., & Amani, A. (2020). A combinational approach towards treatment of breast cancer: An analysis of noscapine-loaded polymeric nanoparticles and doxorubicin. *An Official Journal of the American Association of Pharmaceutical Scientists, 21*(5), 1–12.

Gharsallaoui, A., Saurel, R., Chambin, O., Cases, E., Voilley, A., & Cayot, P. (2010). Utilisation of pectin coating to enhance spray-dry stability of pea protein-stabilised oil-in-water emulsions. *Food Chemistry, 122*(2), 447–454.

Ghibaudo, F., Gerbino, E., Hugo, A. A., Simões, M., Alves, P., Costa, B. F., Orto, V. C. D., Gómez-Zavaglia, A., & Simoes, P. N. (2018). Development and characterization of iron-pectin beads as a novel system for iron delivery to intestinal cells. *Colloids and Surfaces B: Biointerfaces, 170*, 538–543.

Gupta, C., Chawla, P., & Arora, S. (2015). Development and evaluation of iron microencapsules for milk fortification. *CyTA-Journal of Food, 13*(1), 116–123.

Habeych, E., van Kogelenberg, V., Sagalowicz, L., Michel, M., & Galaffu, N. (2016). Strategies to limit colour changes when fortifying food products with iron. *Food Research International, 88*, 122–128.

Hatefi, L., & Farhadian, N. (2020). A safe and efficient method for encapsulation of ferrous sulfate in solid lipid nanoparticle for non-oxidation and sustained iron delivery. *Colloid and Interface Science Communications, 34*, 100227.

Hosny, K. M., Banjar, Z. M., Hariri, A. H., & Hassan, A. H. (2015). Solid lipid nanoparticles loaded with iron to overcome barriers for treatment of iron deficiency anemia. *Drug Design, Development and Therapy, 9*, 313.

Hurrell, R. F. (2021). Iron fortification practices and implications for iron addition to salt. *The Journal of Nutrition, 151*(Supplement_1), 3S-14S.

Jacob, E. M., Borah, A., Jindal, A., Pillai, S. C., Yamamoto, Y., Maekawa, T., & Kumar, D. N. S. (2020). Synthesis and characterization of citrus-derived pectin nanoparticles based on their degree of esterification. *Journal of Materials Research, 35*(12), 1514–1522.

Jafari, S. M., Katouzian, I., Rajabi, H., & Ganje, M. (2017). *Bioavailability and release of bioactive components from nanocapsules* (pp. 494–523). Elsevier.

Jafari, S. M., Vakili, S., & Dehnad, D. (2019). Production of a functional yogurt powder fortified with nanoliposomal vitamin D through spray drying. *Food and Bioprocess Technology, 12*, 1220–1231.

Jash, A., Krueger, A., & Rizvi, S. S. (2022). Venturi-based rapid expansion of supercritical solution (Vent-RESS): Synthesis of liposomes for pH-triggered delivery of hydrophilic and lipophilic bioactives. *Green Chemistry, 24*(13), 5326–5337.

Joel, J., Barminas, J., Riki, E., Yelwa, J., & Edeh, F. (2018). Extraction and characterization of hydrocolloid pectin from goron tula (Azanza garckeana) fruit. *world scientific news,* (101), 157–171.

Jonassen, H., Treves, A., Kjøniksen, A.-L., Smistad, G., & Hiorth, M. (2013). Preparation of ionically cross-linked pectin nanoparticles in the presence of chlorides of divalent and monovalent cations. *Biomacromolecules, 14*(10), 3523–3531.

Kabakci, C., Sumnu, G., Sahin, S., & Oztop, M. H. (2021). Encapsulation of magnesium with lentil flour by using double emulsion to produce magnesium enriched cakes. *Food and Bioprocess Technology, 14*, 1773–1790.

Katuwavila, N. P., Perera, A., Dahanayake, D., Karunaratne, V., Amaratunga, G. A., & Karunaratne, D. N. (2016). Alginate nanoparticles protect ferrous from oxidation: Potential iron delivery system. *International Journal of Pharmaceutics, 513*(1–2), 404–409.

Keawchaoon, L., & Yoksan, R. (2011). Preparation, characterization and in vitro release study of carvacrol-loaded chitosan nanoparticles. *Colloids and Surfaces B, 84*(1), 163–171.

Kiskini, A., Kapsokefalou, M., Yanniotis, S., & Mandala, I. (2012). Effect of iron fortification on physical and sensory quality of gluten-free bread. *Food and Bioprocess Technology, 5,* 385–390.

Kumari, A., & Chauhan, A. K. (2022). Iron nanoparticles as a promising compound for food fortification in iron deficiency anemia: A review. *Journal of Food Science and Technology, 59*(9), 3319–3335.

Mehansho, H. (2006). Iron fortification technology development: New approaches. *The Journal of Nutrition, 136*(4), 1059–1063.

Min, K. A., Cho, J.-H., Song, Y.-K., & Kim, C.-K. (2016). Iron casein succinylate-chitosan coacervate for the liquid oral delivery of iron with bioavailability and stability enhancement. *Archives of Pharmacal Research, 39*, 94–102.

Mishra, R. K., Datt, M., & Banthia, A. K. (2008). Synthesis and characterization of pectin/PVP hydrogel membranes for drug delivery system. *Aaps Pharmscitech, 9*, 395–403.

Mohammadian, M., Waly, M. I., Moghadam, M., Emam-Djomeh, Z., Salami, M., & Moosavi-Movahedi, A. A. (2020). Nanostructured food proteins as efficient systems for the encapsulation of bioactive compounds. *Food Science and Human Wellness, 9*(3), 199–213.

Motwani, S. K., Chopra, S., Talegaonkar, S., Kohli, K., Ahmad, F. J., & Khar, R. K. (2008). Chitosan–sodium alginate nanoparticles as submicroscopic reservoirs for ocular delivery: Formulation, optimisation and in vitro characterisation. *European Journal of Pharmaceutics and Biopharmaceutics, 68*(3), 513–525.

Muthukrishnan, L. (2022). Nanonutraceuticals—Challenges and novel nano-based carriers for effective delivery and enhanced bioavailability. *Food and Bioprocess Technology, 15*(10), 2155–2184.

Nawrocka, A., Szymańska-Chargot, M., Miś, A., Wilczewska, A. Z., & Markiewicz, K. H. (2017). Effect of dietary fibre polysaccharides on structure and thermal properties of gluten proteins–A study on gluten dough with application of FT-Raman spectroscopy, TGA and DSC. *Food Hydrocolloids, 69*, 410–421.

Opanasopit, P., Apirakaramwong, A., Ngawhirunpat, T., Rojanarata, T., & Ruktanonchai, U. (2008). Development and characterization of pectinate micro/nanoparticles for gene delivery. *An Official Journal of the American Association of Pharmaceutical Scientists, 9*(1), 67–74.

Patil, S. S., Khanwelkar, C. C., & Patil, S. (2012). Conventional and newer oral iron preparations. *International Journal Medicine of Pharmaceutical Science, 2*16–22.

Perumal, P., Christopher Selvin, P., & Selvasekarapandian, S. (2018). Characterization of biopolymer pectin with lithium chloride and its applications to electrochemical devices. *Ionics, 24*(10), 3259–3270.

Pitarresi, G., Tripodo, G., Cavallaro, G., Palumbo, F. S., & Giammona, G. (2008). Inulin–iron complexes: A potential treatment of iron deficiency anaemia. *European Journal of Pharmaceutics and Biopharmaceutics, 68*(2), 267–276.

Pratap Singh, A., Siddiqui, J., & Diosady, L. L. (2018). Characterizing the pH-dependent release kinetics of food-grade spray drying encapsulated iron microcapsules for food fortification. *Food and Bioprocess Technology, 11*, 435–446.

Saffarionpour, S., & Diosady, L. L. (2021). Multiple emulsions for enhanced delivery of vitamins and iron micronutrients and their application for food fortification. *Food and Bioprocess Technology, 14*, 587–625.

Saffarionpour, S., & Diosady, L. L. (2022). Delivery of ferric sodium EDTA by water-in-oil-in-water (W1/O/W2) double emulsions: Influence of carrier oil on its in vitro bioaccessibility. *Food and Bioprocess Technology, 15*(2), 421–439.

Seethu, B., Pushpadass, H. A., Emerald, F. M. E., Nath, B. S., Naik, N. L., & Subramanian, K. (2020). Electrohydrodynamic encapsulation of resveratrol using food-grade nanofibres: Process optimization, characterization and fortification. *Food and Bioprocess Technology, 13*, 341–354.

Shilpashree, B., Arora, S., Kapila, S., & Sharma, V. (2020). Whey protein-iron or zinc complexation decreases pro-oxidant activity of iron and increases iron and zinc bioavailability. *Lwt, 126*, 109287.

Shin, G. H., Kim, J. T., & Park, H. J. (2015). Recent developments in nanoformulations of lipophilic functional foods. *Trends in Food Science & Technology, 46*(1), 144–157.

Shubham, K., Anukiruthika, T., Dutta, S., Kashyap, A., Moses, J. A., & Anandharamakrishnan, C. (2020). Iron deficiency anemia: A comprehensive review on iron absorption, bioavailability and emerging food fortification approaches. *Trends in Food Science & Technology, 99*, 58–75.

Sriamornsak, P. (2011). Application of pectin in oral drug delivery. *Expert Opinion on Drug Delivery, 8*(8), 1009–1023.

Wang, Q., Zhang, L., Ding, W., Zhang, D., Reed, K., & Zhang, B. (2020). Orthogonal optimization and physicochemical characterization of water-soluble gelatin-chitosan nanoparticles with encapsulated alcohol-soluble eugenol. *Food and Bioprocess Technology, 13*, 1024–1034.

Yan, J.-K., Qiu, W.-Y., Wang, Y.-Y., & Wu, J.-Y. (2017). Biocompatible polyelectrolyte complex nanoparticles from lactoferrin and pectin as potential vehicles for antioxidative curcumin. *Journal of Agriculture and Food Chemistry, 65*(28), 5720–5730.

Yu, C.-Y., Cao, H., Zhang, X.-C., Zhou, F.-Z., Cheng, S.-X., Zhang, X.-Z., & Zhuo, R.-X. (2009). Hybrid nanospheres and vesicles based on pectin as drug carriers. *Langmuir, 25*(19), 11720–11726.

Yu, Y.-T., Peng, J.-H., Liu, B.-G., Chen, G., & Srinivasakannan, C. (2013). Investigation on preparation of micro-sized hematite powder from hydrous ferrous sulfate using microwave and conventional heating. *High Temperature Materials and Processes, 32*(3), 303–308.